Detection of Oscillatory Modes in Power Systems using Empirical Wavelet Transform

Ambreen Khurram
Dept. of Electronic and Electrical Eng.
University of Leeds, UK
elakh@leeds.ac.uk

Arief Gusnanto
School of Mathematics
University of Leeds, UK
A.Gusnanto@leeds.ac.uk

Petros Aristidou
Dept. of Elec. & Comp. Eng. & Informatics
Cyprus University of Technology, Cyprus
petros.aristidou@cut.ac.cy

***Abstract*—In electric power systems, detecting inter-area oscillations is crucial to the system operators for maintaining the security of the grid – especially in the case of unstable oscillatory behaviour. However, extracting information from unstable, noisy, signals is complicated with conventional signal processing tools suffering from insufficient adaptability. In this paper, we propose a method based on Empirical Wavelet Transform (EWT) to estimate in real-time the dominant inter-area modes in electricity grids. EWT extracts the inherent modulation information by decomposing the signal into its mono components under an orthogonal basis. The instantaneous amplitude and instantaneous frequency is estimated by applying Hilbert transform from the narrow band components of the decomposed EWT signal. The performance of the proposed method is demonstrated using the Nordic test system.**

***Index Terms*—Oscillatory instability, inter-area oscillations, Empirical Wavelet Transform, Hilbert Transform, PMU.**

I. Introduction

Inter-area oscillations are closely related to the small-signal stability of electric power systems. Variations in the system can excite natural frequencies and lead to oscillations. This phenomenon is more prominent in weakly interconnected power system with these oscillations in the range of 0.1 Hz to 1 Hz. In addition, forced oscillations might also occur due to bad controller tuning or malicious operations in the system. In both cases, if the oscillations are not appropriately damped, they can result in increased losses, undue stress on the mechanical components of generators, and in extreme cases to instability [1]. It is therefore important for system operators to have in place real-time monitoring algorithms for detecting and analyzing such events. The advent of phasor measurement units (PMUs) and other real-time measurement methods in electricity grids has made it easier to design data-driven online detection methods.

Various measurement-based methods have been proposed for early diagnostics of inter-area oscillations. Many modal analysis methods use pre-determined basis to process data and are therefore considered as non-adaptive or rigid. Existing methods for inter-area oscillation analysis include Fourier transform [2], continuous wavelet transform [3], Prony's method [4], [5] Matrix Pencil method [6], Kalman filter [7] and total least square [8].

978-1-6654-3597-0/21/$31.00 ©2021 IEEE

Most of the above methods work well with linear data, but their performance deteriorates when the data is non-linear and non-stationary. Furthermore these methods are inflexible as they require prior knowledge of the signal to form a basis function. Any approach with apriori basis could not fit well to the variety of the data from different underlying distributions [9]. In contrast, adaptive decomposition methods adjust to the transient features and emphasise the local characteristics of the signals, without requiring any priori basis to match the signal characteristics. Thus, they can adaptively extract the constituent oscillation modes of mono-component nature [10]. Examples of adaptive decomposition methods include Empirical Mode Decomposition (EMD) [9], Variational Mode Decomposition (VMD) [11], Local Mean Decomposition (LMD) [12] and more recently Empirical Wavelet Transform (EWT) [13].

One of the most promising methods in terms of accuracy and adaptability is EWT. It is able to detect all the local maxima of the frequency spectrum, then get the boundaries (midpoint of two consecutive maxima) to segment the Fourier spectrum. However, as mentioned in [14], it is challenging to employ Fourier spectrum analysis for determining the boundaries in noisy and non-stationary signals. Another problem associated with EWT boundary detection method is selecting the number of bounds in advance. In power systems, there is a large number of closely spaced low-frequency oscillations making it difficult to apriori guess the number of modes in a signal. In [15], the authors proposed a solution to detect the boundaries of the Fourier spectrum using the sliding window approach. However, using just the sliding window technique results in unnecessary segmentation and is computationally expensive.

The decomposed EWT modes satisfy the requirements of mono-component signals and can be used with the Hilbert Transform (HT) to get the instantaneous frequency (IF) representation. The analytical signal constructed from HT allows to extract the instantaneous amplitude (IA) or envelop and the damping Ratio (DR) of each mono-component. From HT the average DR can also be calculated however, the most common way of calculating the DR depends on first and second derivatives, which introduces discontinuities.

Motivated by these existing issues, this paper proposes an online method to estimate in real-time the frequency and DR of oscillatory modes in electric power systems. The detection

methodology based on the EWT, is enhanced to automatically determine the boundaries of the Fourier segments by using a sliding window approach and then limiting the number of segments with a threshold value to control the number of modes. Then, HT is used to extract the frequency and DR of the modes. The contributions of this paper can be summarized as follows:

- We propose an adaptive EWT-based method for real-time detection of oscillatory modes in electric power systems.
- We enhance EWT to automatically determine the boundaries of Fourier segments using a window-based segmentation of Fourier spectrum.
- We improve the accuracy of the average DR estimation by applying logarithmic decrements on the IA without introducing or spreading discontinuities.

The paper is organised as follows. Section II presents the overall algorithm and the proposed methodology. Section III presents some numerical results to verify the performance of the proposed methods. Conclusions are provided in Section IV.

II. Methodology

The proposed framework is intended for real-time automatic modal analysis of multi-dimensional PMU measurements. It is assumed that the real-time, noisy, PMU data are collected at the Supervisory Control and Data Acquisition (SCADA) system and the algorithm is able to extract the existence of oscillatory modes, their frequency, and DR. In case of unstable or badly damped modes, an alarm is raised. Fig. 1 presents the overview of the different steps involved in this analysis – detailed below.

A. Online implementation considerations

Due to the large amount of PMU streaming data, online analysis becomes computationally challenging. It is therefore necessary to apply a diamensionality reduction method before analysing the data. PCA is such a technique, frequently used in electric power system applications. The voltage data matrix to be analyzed by PCA is represented as $\mathbf{X}_{(s\times m)}$, consisting of s observations obtained from the online measurements of the voltage variables $m (m \ll s)$ measured over time t. The matrix $\mathbf{X}$ can be decomposed via singular value decomposition (SVD), $\mathbf{X} = \mathbf{UDV}^T$. Where $\mathbf{U} \in R^{(s\times s)}$ and $\mathbf{V} \in R^{(m\times m)}$ are unitary orthogonal matrices. The diagonal matrix $\mathbf{D} \in R^{(s\times m)}$, contains singular values of decreasing magnitude $(\lambda_1 \geq \lambda_2 \geq, \ldots, \geq \lambda_m)$. If the elements of matrix $\mathbf{X}$ are standardised, a correlation matrix $\mathbf{C(X)} = \mathbf{V\Sigma V}^T$ can be obtained by squaring $\mathbf{D}$ and dividing by $(n-1)$. Similar to $\mathbf{D}$, matrix $\mathbf{\Sigma}$ is also a diagonal matrix and provides variance of $\mathbf{X}$, in which $\sigma_1^2 \geq \sigma_2^2, \ldots, \sigma_m^2 \geq 0$.

The relationship between the PCs, $\mathbf{Y}(\mathbf{y}_1, \mathbf{y}_2, \ldots, \mathbf{y}_m)$ and the original dataset $\mathbf{X}(s \times m)$ is expressed as $\mathbf{Y} = \mathbf{XV} = \mathbf{UD}$. The quotient $(\sum_{q=1}^{k} \lambda_q)/(\sum_{q=1}^{m} \lambda_q) = 0.90$ is used to determine the dimensionality of the system under consideration as it describes the contribution of the k-th PC on the variance of the data. By keeping only k components, the original dataset can be reduced to lower dimensions $y_k(t)$, where $(k \leq m)$.

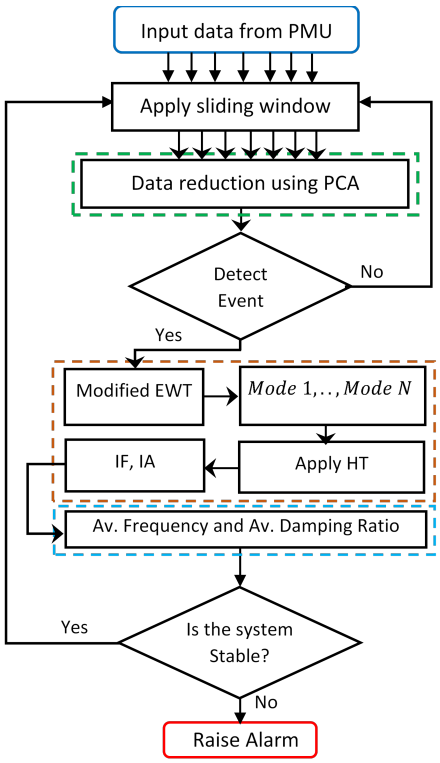

Fig. 1. Flow diagram of the proposed methodology.

Due to the online nature of the detection algorithm, a sliding window analysis must be employed. If we assume that the event causing the oscillatory behaviour happens at time t_d, the sliding window will gradually move from the pre-event data to the area of interest (oscillatory). This transition gives rise to erroneous calculations where the algorithm output is not accurate. To eliminate this problem, we split the algorithm into two stages. First, the algorithm is initialized in standby where the sliding window is monitored to detect the initiation of an event or disturbance. When the event is detected, then the window is reset (to eliminate the pre-event data) and the algorithm goes into the modal analysis stage as soon as the window buffer is full. The disturbance is detected by the employing the event detection method described in [16].

B. Empirical Wavelet Transform

To calculate instantaneous parameters, the individual oscillatory modes present in the signal should be separated from each other (mono-component). The main idea in EWT is to segment the frequency spectrum and then build a series of wavelet filters capable of extracting the mono-components from the signal. The steps required to analyse the real-signal are as follows:

Step 1) Apply fast Fourier transform to the discrete signal $y(t)$ of the sliding window to obtain the frequency spectrum in the range of $[0, \pi]$.

Step 2) Let Fourier spectrum support be divided into N contiguous segments, then $N-1$ boundaries need to be

extracted excluding 0 and π. To find the boundaries, we detect the local maxima L_n in the Fourier spectrum and obtain their corresponding frequency ω_n, where $n = 1, 2, \ldots, N$.

Step 3) The boundary Ω_n between two segments is then defined as the centre of two consecutive maxima:

$$\Omega_n = \frac{\omega_n + \omega_{n+1}}{2} \tag{1}$$

where ω_n and ω_{n+1} are frequencies with $n = 1, 2, \ldots, N-1$. It should be noted that first (Ω_0) and last (Ω_N) boundary frequencies are 0 and π, respectively.

Step 4) The empirical wavelet can be defined as a band pass filters on each segments of the frequency spectrum. The empirical scaling function $\hat{\phi}_n(\omega)$ and the empirical wavelets $\hat{\psi}_n(\omega)$ are given by:

$$\hat{\phi}_n(\omega) = \begin{cases} 1, & \text{if } |\omega| \leq (1-\gamma)\omega_n \\ \cos(\frac{\pi}{2}\alpha(\gamma, \omega_n)), & \text{if } (1-\gamma)\omega_n \leq |\omega| \leq (1+\gamma)\omega_n \\ 0, & \text{otherwise} \end{cases}$$

$$\hat{\psi}_n(\omega) = \begin{cases} 1, & \text{if } (1+\gamma)\omega_n \leq |\omega| \leq (1-\gamma)\omega_{n+1} \\ \cos(\frac{\pi}{2}\alpha(\gamma, \omega_{n+1})), & \text{if } (1-\gamma)\omega_{n+1} \leq |\omega| \leq (1+\gamma)\omega_{n+1} \\ \sin(\frac{\pi}{2}\alpha(\gamma, \omega_n)), & \text{if } (1-\gamma)\omega_n \leq |\omega| \leq (1-\gamma)\omega_n \\ 0, & \text{otherwise} \end{cases}$$

where $\alpha(\gamma, \omega_n) = \beta(\frac{1}{2\gamma\omega_n}(|\omega| - (1-\gamma)\omega_n))$. The parameter γ ensures that no overlap between two consecutive transitions occur and can be selected as $\gamma < min_n\left(\frac{\omega_{n+1}-\omega_n}{\omega_{n+1}+\omega_n}\right)$.

$\beta(x)$ is an arbitrary function defined as

$$\beta(x) = \begin{cases} 0, & \text{if } x \leq 0 \\ 1, & \text{if } x \geq 1 \\ \beta(x) + \beta(1-x) = 1, & \forall\ x \in [0, 1] \end{cases} \tag{2}$$

Step 5) Having defined the empirical wavelet and scaling function, the empirical wavelet transforms $W_y^\epsilon(n, t)$ of the signal is defined in a way similar to the classic wavelet transform. The approximate coefficients can be expressed as the inner product of analysed signal $y(t)$ with scaling function:

$$W_y^\epsilon(0, t) = \langle y, \phi_1 \rangle = \int y(\tau)\overline{\phi_1(\tau - t)}dt = (\hat{y}(\omega)\overline{\hat{\phi_1}(\omega)})^\vee$$

In the same way, the detailed coefficients are obtained by the inner product of analysed signal $y(t)$ with empirical wavelets:

$$W_y^\epsilon(n, t) = \langle y, \psi_n \rangle = \int y(\tau)\overline{\hat{\psi}_n(\tau - t)}dt = (\hat{y}(\omega)\overline{\hat{\psi}(\omega)})^\vee$$

where $W_y^\epsilon(n, t)$ denotes the detailed coefficients at time t for the n filter bank. $\phi_1(\omega)$ and $\psi(\omega)$ are empirical wavelet function and empirical scaling function respectively. $\hat{\phi}_1(\omega)$ and $\hat{\psi}(\omega)$ are Fourier transform of $\phi_1(\omega)$ and $\psi(\omega)$ which are defined by (II-B) and (II-B). The reconstructed signal can be obtained by:

$$y(t) = W_y^\epsilon(0, t)^* \phi_1(t) + \sum_{n=1}^{N} W_y^\epsilon(n, t)^* \phi_n(t) \tag{3}$$

The empirical mode $y_n(t)$ can be given by:

$$\begin{aligned} y_0(t) &= W_y^\epsilon(0, t)^* \phi_1(t) \\ y_n(t) &= W_y^\epsilon(n, t)^* \psi_n(t) \end{aligned} \tag{4}$$

C. Proposed Segmented Empirical Wavelet Transform

To enable the automatic detection of boundaries for the adaptive decomposition of EWT, we propose the window based Segmented Empirical Wavelet Transform (SEWT) for mode separation. A drawback of EWT is that when the analysed signal comprised of noise and contain frequencies close to each other some local maxima might appear in the detected peak sequence, which lead to improper segmentation. SEWT divides the Fourier spectrum without being stuck in the local maxima. However, as the window moves along the spectrum, some unnecessary segmentation is produced. Therefore, a threshold is added, which retain peaks as a percentage of the maximum amplitude in the spectrum range. The implementation steps are given below:

1) Consider a real voltage signal $y(t)$, which is sampled at a frequency of F_s. First, we apply FFT on the discrete signal $y(t_d)$ to obtain the frequency spectrum X_ω.
2) Then, we choose a step size as the reciprocal of the Nyquist frequency $\mathcal{N}$ of the signal:

$$S = \frac{1}{\mathcal{N}}, \quad \text{where } \mathcal{N} = \frac{F_s}{2} \tag{5}$$

The step size is chosen as the reciprocal of Nyquist frequency to ensure it is small enough to cover the low frequency range in the inter-area oscillations.
3) We divide the FFT spectrum in segments Λ_n using the step size S:

$$\Lambda_n = X_\omega[j \times S, (j+1) \times S]_{j=1,2,\ldots,p} \tag{6}$$

where p is the length of spectrum X_ω.
4) We find the maximum in each segment $L_{\max} = \{L_1, L_2, ...\}$ and sort them in a decreasing order.
5) We filter the maxima $L_{\max}$ those above a selected threshold α: $L_{\max}^Z = \{L_n \geq \alpha | n = 1, \ldots, N\}$. Where the threshold α determines which peaks are retained as a percentage of the maximum amplitude.
6) Finally, the boundaries are defined as midpoints between two consecutive maxima as in (1).

Fig. 2 shows the segmentation of the Fourier spectrum using SEWT algorithm. The dashed vertical lines represent the detected Fourier boundaries.The most dominant frequencies can be retained by increasing the value of the threshold.

D. Hilbert Transform

The empirical modes are narrow band components, therefore HT can be applied to study the signal's time variability in detail. For a given real signal $y(t)$, the analytical signal $z(t)$ can be given as:

$$z(t) = y(t) + i\mathrm{H}[y(t)] = A(t)e^{i\theta(t)} \tag{7}$$

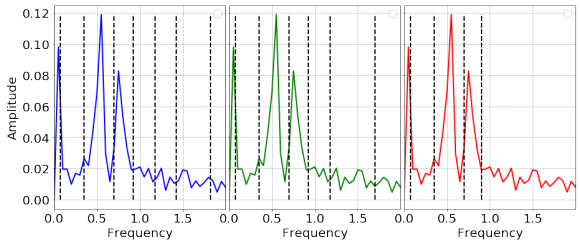

Fig. 2. Segmentation of Fourier spectrum using SEWT, with the threshold values of 0% (blue), 10% (green) and 15% (red) of the maximum amplitude.

where $A(t)$ represents IA envelop, $\theta(t)$ is the instantaneous phase (IP) and H$[y(t)]$ is the HT of $y(t)$ and is defined using Cauchy principal value $p.v.$ as:

$$\mathrm{H}[y(t)] = \frac{1}{\pi} p.v. \int_{-\infty}^{+\infty} \frac{y(\tau)}{t-\tau} d\tau \tag{8}$$

In terms of $y(t)$ and its HT, the IA, IP and IF are defined as:

$$\mathrm{IA} = A(t) = \sqrt{y^2(t) + \mathrm{H}[y(t)]^2} \tag{9}$$

$$\mathrm{IP} = \theta(t) = tan^{-1}\left(\frac{\mathrm{H}[y(t)]}{y(t)}\right) \tag{10}$$

$$\mathrm{IF} = f(t) = \frac{1}{2\pi}\frac{d\theta(t)}{dt} \tag{11}$$

The instantaneous damping function $\zeta(t)$ is calculated using the technique provided in [17]:

$$\zeta(t) = \sqrt{\frac{\rho(t)^2}{1+\rho(t)^2}} \tag{12}$$

where

$$\rho(t) = \left| \frac{\ln \frac{\mathrm{IA_0}}{\mathrm{IA(t)}}}{2\pi \cdot \mathrm{IF(t)} \cdot \mathrm{t}} \right| \tag{13}$$

and $\mathrm{IA_0}$ is the initial amplitude.

E. Average parameters

While the average frequency $\mathrm{F_{avg}}$ is calculated by taking the average of (11), to obtain the average damping coefficient, a damping equation (mentioned in[18]) is commonly used. However, it relies on computing the derivative which introduces discontinuities. In this paper, we estimate average DR ζ_{avg} with a combination of a logarithmic decrement and IA envelop obtained from the (9). The most common way to calculate DR of a free decaying oscillation is with:

$$\zeta = \frac{\delta}{\sqrt{(2\pi)^2 + \delta^2}} \tag{14}$$

where δ is the logarithmic decrement of peak amplitudes of two points x_1 and x_2, exactly n cycles apart

$$\delta = \frac{1}{n} \ln \frac{x_1}{x_2} \tag{15}$$

By using (14) and (15) the average DR ζ_{avg} can be estimated much more precisely from successively discrete decaying points of the IA envelop (Fig. 3). First the logarithmic decrement is calculated by replacing the peaks in (14) with each successive sample (n=1) in the envelop and then dividing it by total number of samples s in the window W_0:

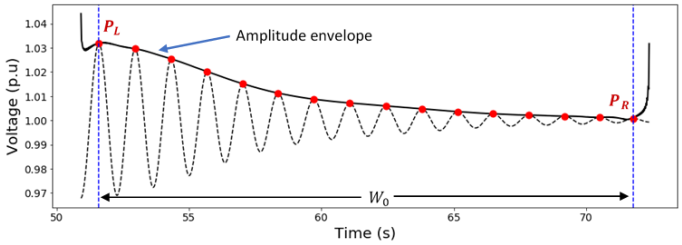

Fig. 3. IA envelop fitted with the reconstructed EWT signal.

$$\delta_i = \frac{(\frac{1}{n} \ln \frac{\mathrm{IA}_i}{\mathrm{IA}_{i+1}})}{s} \tag{16}$$

where $\mathrm{IA_i}$ is the value of IA at the i-th envelop sample. Next the average DR ζ_{avg} is calculated by substituting (16) in (14) and adding all the values:

$$\zeta_{avg} = \sum_{i=1}^{s} \frac{\delta_i}{\sqrt{(2\pi)^2 + \delta_i^2}} \tag{17}$$

III. Numerical Results

A. System model and case study description

The proposed scheme is tested using the Nordic test system [19]. Time-domain simulations were conducted using the dynamic simulation software PyRAMSES [20] and the results were saved in a database, emulating the PMU measurements. Only voltage magnitude measurements are used from the 20 synchronous generators. A window of 20 s sliding with 1 s of new data each time is chosen (19 s overlap).

Two case study scenarios were investigated a) **Stable oscillations model (C1)** and b) **Unstable oscillations model (C2)**. For C2 several generator PSS controllers were deactivated to destabilise the system. In both cases, the modes are excited by applying a three-phase fault at bus 4072 at time $t = 50$ s which is automatically cleared after 100 ms. All the measurements are sampled at 50 Hz. Gaussian white noise is added to the voltage signals with Signal to Noise Ratio (SNR) of 50 dB.

We performed a small-signal stability analysis on the original differential-algebraic model used for the above two cases and identified the main electromechanical modes as detailed in Table I. These are used as a benchmark (BM) for our real-time detection algorithm that only uses the data flow.

B. Case study 1; Stable Model:

In the first step, PCA is applied to the normalized voltage magnitude data. The first principal component (PC1) accounts for 83% of the variation, while the second component (PC2) accounts for 8% of the total explained variance. Therefore,

TABLE I
Small-signal stability analysis.

	C1		C2		
	Mode2	**Mode3**	**Mode2**	**Mode3**	**Mode4**
Frequency(Hz)	0.538	0.742	0.533	0.766	0.949
DR (%)	3.7	3.9	-0.4	-0.1	0.3

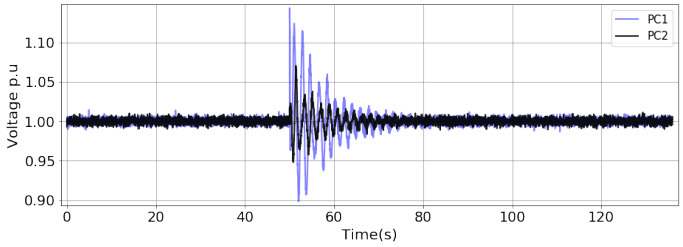

Fig. 4. Case 1: PC1 and PC2 for the 20 generator buses from Nordic-32 test system. PC1 captures 83% of the variation, while the PC2 captures 8% of the total explained variance.

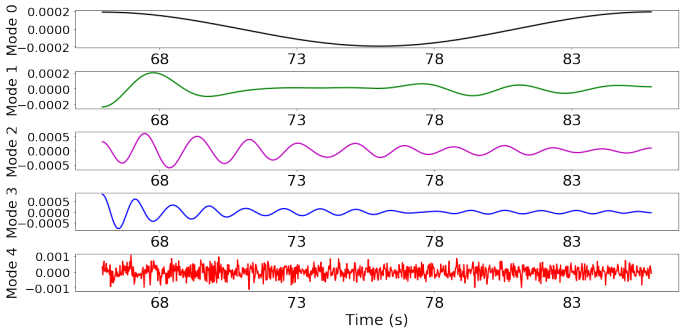

Fig. 5. Case 1: Decomposition of PC1 voltage signal using SEWT.

only the first two PCs are retained since together they capture a total of 91% variation. Fig. 4 shows the reduced signal obtained after applying PCA on 20 voltage buses.

Once the event is detected (see Section II), the compressed PCA signal is decomposed. Fig. 2 shows the results of the segmentation of the Fourier spectrum using three different thresholds α and a step size of 0.04 Hz. Fig. 5 shows the modes extracted using SEWT with the threshold $\alpha = 15\%$. The method analyses all the modes but we only consider Mode-2 and Mode-3 as these modes contain more abundant impulse information. Their corresponding frequencies are estimated 0.54 Hz and 0.77 Hz. The signal power of Mode-0 and Mode-1 is negligible and therefore discarded. Meanwhile, the noise is separated from the dominant components. Therefore, HT is applied to Mode-2 and Mode-3 only.

Fig. 3 shows the decaying amplitude from HT for Mode-2. The envelop obtained from the application of the HT is fitted to the reconstructed EWT signal. At the beginning and end of the time series there is a difference due to the end effect [18] of HT as a result of a finite time series. In a real time, analysis, we have a continuous stream of data therefore to overcome this issue the left and right tails of the IA envelop are discarded without extending the ends. No information is lost as the discarded data is overlapping with the next/previous sliding windows. The average DR and the instantaneous DR of the truncated envelop are computed using (17) and (13).

Fig. 6 shows the corresponding IA and instantaneous DR of the extracted modes using the online estimation approach. The estimated average DR, after application of proposed algorithm, is shown in Fig. 7. When the oscillatory response is initiated, the sliding window moves from the pre-event to the oscillatory data. The output of the SEWT algorithm during

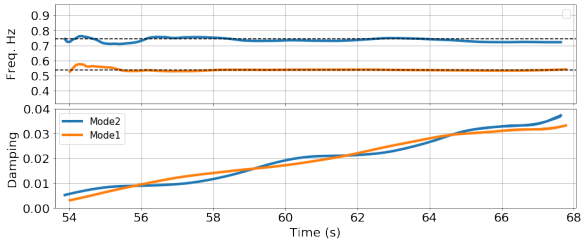

Fig. 6. Case 1: Top panel shows IF $f(t)$ and the bottom panel shows instantaneous DR $\zeta(t)$ of extracted modes from PC1.

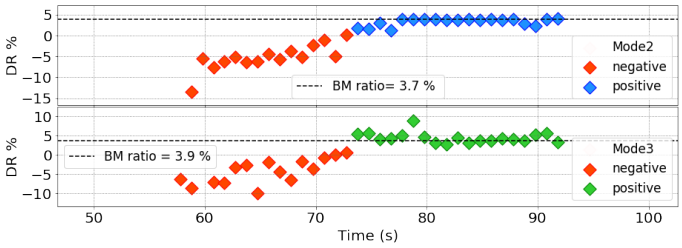

Fig. 7. Case 1: Estimates for the average DR ζ_{avg} from the PC1 during the event. The results are obtained using a 20 seconds sliding window.

this phase would be inaccurate, as shown by the red dots, thus ignored. Using the event detection technique, SEWT will only start reporting when the sliding window moves into the oscillatory zone. Thus, the pre-event results are discarded and the algorithm will only report the ζ_{avg} estimates shown in blue and green for Mode-2 and Mode-3, respectively.

The performance is assessed using the Mean Squared Error (MSE). The estimates of average DR and average frequency for each sliding window are compared with the BM values from the small-signal analysis. The MSE is found by averaging the squared error over the sampled window length. Table II provides the results of the MSE for SEWT compared to EWT and VMD. SEWT PC1 and SEWT PC2 indicate the results obtained from the PC1 and PC2, respectively. Correlation analysis of the PCs suggest that PC1 is positively correlated with all the twenty generators except g4. Thus, there is a direct relation between all the voltage buses and all of them participate in the oscillations. PC2 has large negative associations with busses g1, g2, g19, and g20, therefore the larger part of variations are coming from them. Further analysis of the voltage variables indicates that the negatively correlated generators mainly contribute to the strong 0.54 Hz mode while the rest of generators contribute to the 0.54 Hz mode and a weak 0.77 Hz mode. This mode is vaguely visible in the PC2 as reflected by the high MSE of the DR ζ_{avg} in Table II.

C. Case study 2; Unstable Model:

For C2 the voltage response of the system is displayed in Fig. 8. The total variance accounts for 93% of the information (85% for PC1 and 8% for PC2). Note that with this disturbance, in addition to Mode-1 and Mode-2 discussed in case C1 there is also another mode detected around 0.9 Hz. Analysis of the voltage variables for C2 indicates that these modes are visible in all the busses. Therefore these modes are adequately captured by both PCs leading to a low MSE in Table II.

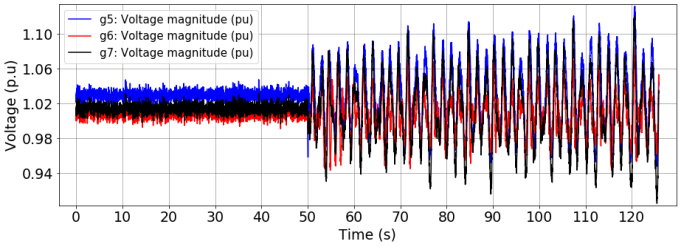

Fig. 8. Case 2: Temporal evolution of voltage signals.

Fig. 9 shows the SEWT estimation of the average DR and average oscillation frequency for case C2. The red dots highlight the negative DR and the blue dots indicate that the DR estimates are positive. It can be seen from Fig. 9 that the algorithm tracks the actual DR of the mode dynamically throughout the disturbance. These results show that the proposed methodology can provide valuable feedback on the evolving status of the DR level of the oscillatory mode to the operator during this complex disturbance process.

IV. Conclusion

This paper describes the real-time application of a proposed EWT-based technique for estimating the modal frequency and DR. The algorithm is highly adaptive to the signal's oscillation characteristics. The proposed SEWT method automatically estimates the number of modes based on the frequency contents of the signal. The window-based automatic mode detection method locates the local maxima, and the use of amplitude threshold avoids any unnecessary segmentation of the Fourier spectrum. Unlike conventional single-channel methods, the proposed algorithm is based on multi-variate data analysis and captures the global dynamic features. In addition, through data compression, it is effective in reducing noise errors. Test result evaluation and comparison with existing methods reveal that the proposed method shows excellent potential for real-time monitoring and identification of inter-area oscillations.

References

[1] J. Machowski, J. Bialek, and J. Bumby, *Power system dynamics: stability and control*. JohnWiley and Sons, 2008.

[2] K. C. Lee and K. P. Poon, "Analysis of power system dynamic oscillations with beat phenomenon by fourier transformation," *IEEE Trans. on Power Systems*, 1990.

TABLE II
Test result for simulation cases

Method	Mode	C1 MSE		C2 MSE	
		FREQ	DR	FREQ	DR
VMD	*Mode-2*	0.058	0.629	0.040	0.040
	Mode-3	0.629	1.876	0.013	0.110
	Mode-4	-	-	0.005	0.295
EWT	*Mode-2*	0.024	1.041	0.053	0.905
	Mode-3	0.088	2.447	0.007	0.551
	Mode-4	-	-	0.013	3.168
SEWT PC1	*Mode-2*	0.001	0.144	0.060	0.092
	Mode-3	0.010	1.059	0.001	0.535
	Mode-4	-	-	0.001	0.150
SEWT PC2	Mode-2	0.009	1.269	0.001	0.318
	Mode-3	0.020	2.126	0.006	0.857
	Mode-4	-	-	0.147	0.860

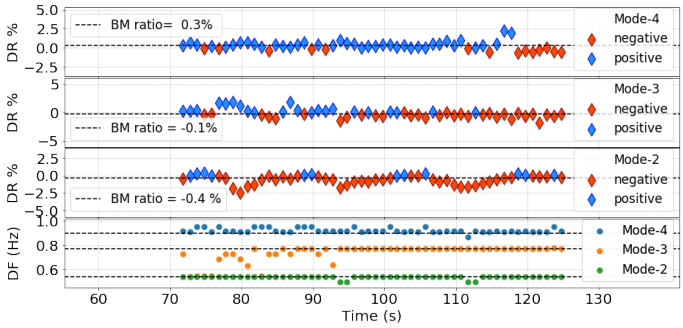

Fig. 9. Case 2: Estimates of average DR ζ_{avg} and average frequency $\mathrm{F_{avg}}$ from PC1.

[3] F. Shiri and B. Mohammadi-Ivatloo, "Identification of inter-area oscillations using wavelet transform and phasor measurement unit data," *Intern. Trans. on Electr. Energy Systems*, vol. 25, no. 11, pp. 2831–2846, 2015.

[4] C. J. Demeure and L. L. Scharf, "Initial results in prony analysis of power system response signals," *IEEE Trans. on Power Systems*, 1990.

[5] J. F. Hauer, "Application of prony analysis to the determination of modal content and equivalent models for measured power system response," *IEEE Trans. on Power Systems*, 1991.

[6] M. L. Crow and A. Singh, "The matrix pencil for power system modal extraction," *IEEE Trans. on Power Systems*, 2005.

[7] R. A. Wiltshire, G. Ledwich, and P. O'Shea, "A Kalman filtering approach to rapidly detecting modal changes in power systems," *IEEE Trans. on Power Systems*, vol. 22, pp. 1698–1706, nov 2007.

[8] J. M. Papy, L. De Lathauwer, and S. Van Huffel, "Common pole estimation in multi-channel exponential data modeling," *Signal Processing*, 2006.

[9] N. E. Huang, Z. Shen, S. R. Long, M. C. Wu, H. H. Snin, Q. Zheng, N. C. Yen, C. C. Tung, and H. H. Liu, "The empirical mode decomposition and the Hubert spectrum for nonlinear and non-stationary time series analysis," *Proceedings of the Royal Society A: Mathematical, Physical and Engineering Sciences*, vol. 454, no. 1971, pp. 903–995, 1998.

[10] Z. Feng, D. Zhang, and M. J. Zuo, "Adaptive Mode Decomposition Methods and Their Applications in Signal Analysis for Machinery Fault Diagnosis: A Review with Examples," *IEEE Access*, 2017.

[11] K. Dragomiretskiy and D. Zosso, "Variational mode decomposition," *IEEE Trans. on Signal Processing*, vol. 62, pp. 531–544, feb 2014.

[12] J. S. Smith, "The local mean decomposition and its application to EEG perception data," *J R Soc Interface*, vol. 2, no. 5, pp. 443–454, 2005.

[13] J. Gilles, "Empirical wavelet transform," *IEEE Trans. on Signal Processing*, vol. 61, no. 16, pp. 3999–4010, 2013.

[14] J. P. Amezquita-Sanchez and H. Adeli, "A new music-empirical wavelet transform methodology for time-frequency analysis of noisy nonlinear and non-stationary signals," *Digital Signal Processing: A Review Journal*, 2015.

[15] S. Dong, M. Yuan, Q. Wang, and Z. Liang, "A modified empirical wavelet transform for acoustic emission signal decomposition in structural health monitoring," *Sensors (Switzerland)*, 2018.

[16] D. Q. Zhou, U. D. Annakkage, and A. D. Rajapakse, "Online monitoring of voltage stability margin using an artificial neural network," *IEEE Trans. on Power Systems*, vol. 25, pp. 1566–1574, aug 2010.

[17] R. I. Ramírez and L. A. Montejo, "On the identification of damping from non-stationary free decay signals using modern signal processing techniques," *Intern. Journal of Advanced Structural Engineering*, 2015.

[18] D. S. Laila, A. R. Messina, and B. C. Pal, "A refined Hilbert-Huang transform with applications to interarea oscillation monitoring," *IEEE Trans. on Power Systems*, 2009.

[19] T. Van Cutsem, M. Glavic, W. Rosehart, C. Canizares, M. Kanatas, L. Lima, F. Milano, L. Papangelis, R. A. Ramos, J. A. d. Santos, B. Tamimi, G. Taranto, and C. Vournas, "Test systems for voltage stability studies," *IEEE Trans. on Power Systems*, vol. 35, no. 5, pp. 4078–4087, 2020.

[20] P. Aristidou, S. Lebeau, and T. Van Cutsem, "Power system dynamic simulations using a parallel two-level schur-complement decomposition," *IEEE Trans. on Power Systems*, vol. 31, no. 5, pp. 3984–3995, 2016.